

Article

Electrochemical Determination of 4-Bromophenoxyacetic Acid Based on CeO₂/eGr Composite

Haijun Du ^{1,†}, Yan Zhang ^{1,†}, Xin Wang ^{1,2}, Huali Hu ¹, Jixing Ai ¹, Huanxi Zhou ^{2,3}, Xia Yan ³, Yang Yang ^{2,*} 
and Zhiwei Lu ^{4,*}

¹ School of Chemical Engineering, Guizhou Minzu University, Guiyang 550025, China

² School of Materials Science and Engineering, Guizhou Minzu University, Guiyang 550025, China

³ School of Mechatronics Engineering, Guizhou Minzu University, Guiyang 550025, China

⁴ College of Science, Sichuan Agricultural University, Ya'an 625014, China

* Correspondence: y.yang@gzmu.edu.cn (Y.Y.); zhiweilu@sicau.edu.cn (Z.L.)

† These authors contributed equally to this work.

Abstract: The determination of plant growth regulators is of great importance for the quality monitoring of crops. In this work, 4-bromophenoxyacetic acid (4-BPA), one of the phenoxyacetic acids, was detected via the electrochemical method for the first time. A CeO₂-decorated electrochemical exfoliated graphene (eGr) composite (CeO₂/eGr) was constructed as the sensor for sensitive detection of 4-BPA due to the synergistic effect of the excellent catalytic active sites of CeO₂ and good electron transference of the eGr. The developed CeO₂/eGr sensor displayed a good linearity in a wide range from 0.3 to 150 μmol/L and the lowest detection limit of 0.06 μmol/L for 4-BPA detection. Electrochemical oxidation of 4-BPA follows a mix-controlled process on the CeO₂/eGr electrode, which involves 2e in the transference process. This developed CeO₂/eGr sensor has excellent repeatability with a relative standard deviation (RSD) of 2.35% in 10 continuous measurements. Moreover, the practical application of the sensor for 4-BPA detection in apple juice has recoveries in the range of 90–108%. This proposed CeO₂/eGr sensor has great potential for detecting plant growth regulators in the agricultural industry.



Citation: Du, H.; Zhang, Y.; Wang, X.; Hu, H.; Ai, J.; Zhou, H.; Yan, X.; Yang, Y.; Lu, Z. Electrochemical Determination of 4-Bromophenoxyacetic Acid Based on CeO₂/eGr Composite. *Biosensors* **2022**, *12*, 760. <https://doi.org/10.3390/bios12090760>

Received: 30 August 2022

Accepted: 13 September 2022

Published: 15 September 2022

Publisher's Note: MDPI stays neutral with regard to jurisdictional claims in published maps and institutional affiliations.



Copyright: © 2022 by the authors. Licensee MDPI, Basel, Switzerland. This article is an open access article distributed under the terms and conditions of the Creative Commons Attribution (CC BY) license (<https://creativecommons.org/licenses/by/4.0/>).

Keywords: plant growth regulators; 4-bromophenoxyacetic acid; electrochemical determination; lowest detection limit; CeO₂/eGr composite

1. Introduction

Plant growth regulators (PGRs) are widely used to promote a crop's productivity and quality [1,2], control crop type [3], resist biotic and abiotic stress [4], regulate differentiation of cells, control weeds [5], and for phytoremediation [6]. 4-bromophenoxyacetic acid (4-BPA) is a PGR that can control weeds, accelerate plant growth, and enhance the fruit setting rate. However, inappropriate usage of 4-BPA will cause malformations and affect the quality of the crop. Furthermore, accumulation in the crop can be a detriment to other plants, animals, and to human health. Therefore, it is of great necessity to develop convenient, sensitive, and reliable analytical methods for 4-BPA determination. Unfortunately, to the authors' knowledge, only Sutcharitchan [7] has developed a liquid chromatography-tandem mass spectrometry (LC-MS) method for 4-BPA determination in Chinese herbs.

4-BPA is a phenoxyacetic acid, and a variety of analytical methods for phenoxyacetic acid detection have been developed, including capillary electrophoresis with laser-induced fluorescence [8], ultra-high liquid chromatography-mass spectrometry [9], headspace gas chromatography high-performance liquid chromatography [10] and electrochemical methods [11–15]. Compared to these methods, electrochemical methods have the advantage of high sensitivity, low cost, portability, and simple operation [16,17]. The direct interaction between the electrode surface and analyte can reduce the lowest limitation and improve the detection range, which has the potential to establish a rapid on-site inspection

method. In addition, the advantages of the electrochemical sensors include fast response, on-site deployment, effective detection without sample pretreatment and the modified nanocomposite exhibits high electrocatalytic activity for an analyte [18]. Because of its electrochemical activity, 4-BPA is detectable via electrochemical methods.

Ceria (CeO_2) is an n-type semiconductor that has the potential to be used as a sensing material, since it has excellent redox characteristics and is highly catalytic, biocompatible, and non-toxic [19,20]. Moreover, CeO_2 can selectively bind with organic molecules due to its characteristics of oxygen vacancies, free electrons, and high chemical stability [21]. However, it is hard to directly use as modifier material in electrochemical sensors as CeO_2 suffers from poor conductivity and easy aggregation. Therefore, it is essential to enhance its sensing activities by introducing conductive support.

Graphene (Gr) is one of the best candidates for the construction of electrochemical sensors, as it has unique and extraordinary physical and chemical properties, such as high specific surface area, low charge-transfer resistance, excellent electrochemical activity and high electrical conductivity [22,23], which improve the value of heterogeneous electron transfer (HEF) and the output signal intensity [24,25]. Over the past few decades, different protocols, including top-down approach (e.g., chemical vapor deposition) and bottom-up methods (e.g., electrochemical exfoliation) have been developed [26,27]. Among these methods, electrochemical exfoliation of graphite has the advantages of being low-cost and environmentally friendly, easily made and scalable, and the electrochemical conditions are controllable. Moreover, the exfoliated graphene is a zero-gap semiconductor; it can be doped with p-block elements (N, S, P, B, and metal oxides) and d-block elements (inherent impurities) [26,28] to improve the HEF to promote the interaction between target molecules and the electrode. In the study of Liu [29], gold-palladium nanoparticles were cast on the graphene nano-platelets, and the nanocomposites showed high electrocatalytic ability towards the oxidation of hydrazine. Li [30] synthesized three kinds of CeO_2 nanostructures and then loaded them on the graphene nanoplatelets to detect phenolic pollutants, which exhibited excellent electrochemical activity. Previously, our group has developed an electrochemical exfoliation graphene (eGr) sensor, which displayed the lowest detection limit (LOD) of $0.15 \mu\text{M}$ for electrochemical determination of Kinetin [31]. Therefore, CeO_2 was decorated on the surface of eGr to form a nanocomposite that will have a synergetic effect between eGr and CeO_2 , thus forming a sensitive, selective and promising electrode system for 4-BPA detection. In the electrochemical determination process, several types of electrodes are suitable for electroanalytical applications, such as glassy carbon electrodes (GCE), gold electrodes (GE), carbon paste electrodes (CPE) and pencil electrodes. Among these electrodes, GCE shows attractive electrochemical reactivity, negligible porosity, good mechanical rigidity and good repeatability and reproducibility [32].

Herein, CeO_2 nanocubes were synthesized via the hydrothermal method and electrochemical exfoliated graphene was prepared through the previous method [25]. A CeO_2 decorated eGr composite was constructed and employed to detect 4-BPA for the first time. This developed eGr/ CeO_2 sensor has a linear range from 0.3 to $150 \mu\text{M}$ and the LOD of $0.06 \mu\text{M}$ for 4-BPA determination, which shows great potential for the detection of plant regulators in the agricultural industry.

2. Materials and Methods

2.1. Reagents and Materials

All reagents used in the experiments are analytical reagent grade and without any treatment. Graphite sheets were purchased from the local electronic market. $\text{Ce}(\text{NO}_3)_3 \cdot 6\text{H}_2\text{O}$, 4-BPA, indole 3-acetic acid, naphthalene acetic acid and 6-benzylaminopurine were purchased from Macklin biochemical Technology Co., Ltd. (Shanghai, China). A solution of 0.1 M 4-BPA was prepared by dissolving a suitable amount of 4-BPA in alcohol and diluting the mixture to 10 mL , then the solution was stored in a refrigerator at $4 \text{ }^\circ\text{C}$. Phosphate buffer solution (PBS) was used as a supporting electrolyte by combining a stock solution of 0.1 M KH_2PO_4 (Aladdin Reagent Co., Ltd., Shanghai, China) and 0.1 M NaH_2PO_4 (Aladdin

Reagent Co., Ltd., Shanghai, China), then 0.1 M H_3PO_4 (Aladdin Reagent Co., Ltd., Shanghai, China) and 0.1 M NaOH (Sinopharm Group Chemical Reagent Co., Ltd., Shanghai, China) were, respectively, used to adjust the pH to the desired value.

2.2. Preparation of CeO_2 , eGr, and eGr/ CeO_2 Composites

CeO_2 nanocubes were prepared using the hydrothermal method. Firstly, 0.6948 g $\text{Ce}(\text{NO}_3)_3 \cdot 6\text{H}_2\text{O}$ and 0.0224 g hexamethylenetetramine (HMT) was dissolved in 40 mL distilled water and 40 mL ethanol. The resulting solution was vigorously stirred for 20 min at room temperature, then it was transferred into a 100 mL Teflon-lined stainless-steel autoclave, and hydrothermally heated at 180 °C for 20 h. After that, the product was collected by centrifuging, and alternatively washed with distilled water and ethanol to a neutral pH, and then dried in an oven at 80 °C for 12 h. Finally, the obtained yellow powder was calcined at 400 °C for 5 h.

For eGr preparation, a two-electrode cell was used including graphite foil as an anode, a platinum net as a cathode, and 0.1 M $(\text{NH}_4)_2\text{SO}_4$ as a supporting electrolyte, whereas the eGr was obtained with the aid of SO_4^{2-} intercalation and oxidization to produce sulfur dioxide and oxygen gases, then the product was centrifuged, filtrated and dried overnight.

Next, 9 mg CeO_2 and/or 9 mg eGr were dispersed in 9 mL *N,N'*-dimethylformamide (DMF) solution with vigorous stirring and then ultra-sonicating for 2 h to obtain the CeO_2 , eGr, and CeO_2 /eGr suspensions. The glassy carbon electrodes (GCEs) were polished to a mirror-like surface with 0.3 and 0.5 μm Al_2O_3 slurries on chamois leather, then alternately rinsing with distilled water/ethanol (1:1, *v/v*) solution and double distilled water for 3 min. Finally, CeO_2 , eGr, and CeO_2 /eGr suspensions were, respectively, drop-coated on the mirror-like surface of GCEs to obtain CeO_2 /GCE, eGr/GCE, and CeO_2 /eGr/GCE electrodes.

2.3. Characterization

Scanning electron microscope (SEM, Thermo scientific Apreo 2C, Waltham, MA, USA) and transmission electron microscope (TEM, FEI Tecnai F20, Hillsboro, OR, USA) and High-resolution transmission electron microscope (HRTEM, FEI Tecnai F20, Hillsboro, OR, USA) were used to analyze the surface morphologies of CeO_2 , eGr and CeO_2 /eGr nanocomposite. Raman spectra were collected with a 532 nm diode laser by Thermo Fisher Dxr2xi (Waltham, MA, USA). X-ray diffraction (XRD) patterns were recorded by the PANalytical Empyrean system (Almelo, The Netherlands). X-ray photoelectron spectra (XPS) were recorded by Thermo Scientific K-Alpha (Waltham, MA, USA).

Cyclic voltammetry (CV), linear sweep voltammetry (LSV), and differential pulse voltammetry (DPV) measurements were performed on a CHI 660E electrochemical workstation (CH Instruments ins., Shanghai, China) and a classic three-electrode system. CVs were carried out with the potential range from 0.8 to 1.5 V at a scan rate of 0.1 V s^{-1} . LSVs were carried out with the potential range from 0.9 to 1.6 V at a scan rate of 0.1 V s^{-1} . DPVs were carried out from 0.8 to 1.5 V with parameters of 0.05 V amplitude, 0.06 s pulse width, 0.02 s sampling width, 0.5 s pulse period and 30 s rest time. A glassy carbon electrode (GCE, diameter 3 mm) or modified GCE as the working electrode, a platinum wire served as a counter electrode and Ag/AgCl was used as the reference electrode.

2.4. Sample Pretreatment

The purchased apple was squeezed into juice (120 g) and the fresh apple juice was mixed with distilled water and sonicated for 20 min (at room temperature), then centrifuged for 5 min with 10,000 r/min to obtain the supernatants. Supernatants were collected for further quantification of 4-BPA.

3. Results and Discussion

3.1. Morphology and Phase Structure Characterization

The morphology of the synthesized CeO_2 was observed by SEM, which presents a nano-cubic structure, and agglomerated together due to the nanosize effect (Figure 1a). The

diffraction rings in the selected area electron diffraction (SAED) suggest the as-synthesized CeO_2 is polycrystalline and mainly exists in (111), (200), (220), and (311) crystallite planes (Figure 1b). From HRTEM (Figure 1c), there is a main lattice space distance of 0.314 nm which belongs to (111) crystallite plane of CeO_2 . For the eGr sample, the TEM image indicates the prepared eGr displays a layered structure (Figure 1d), and the SAED indicates that the eGr mainly presents (002), and (004) crystallite planes (Figure 1e), the existed lattice space distance of 0.34 nm matches well with the theoretical value of graphene (002) crystallite plane (Figure 1f); it verifies the high quality of the prepared eGr. The CeO_2 /eGr nanocomposite used here was 1:1 in a weight ratio (1:1 wt.). Figure 1g shows that CeO_2 is uniformly loaded on the surface of eGr and forms on the selected area (Figure 1h); the corresponding elemental mapping illustrates that the elements of C, O and Ce exist in the CeO_2 /eGr nanocomposite (Figure 1i–k).

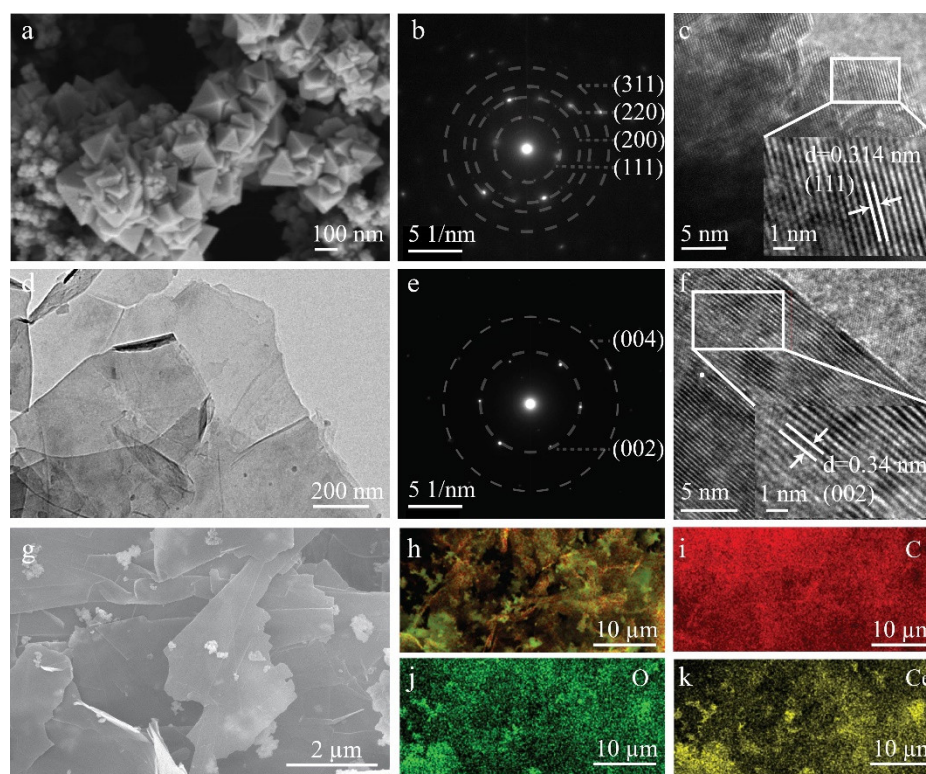


Figure 1. SEM image (a), SEAD (b) and HRTEM (c) of CeO_2 , TEM (d), SEAD (e) and HRTEM (f) of eGr, SEM image (g) and corresponding elemental mapping of the selected area (h), C (i), O (j) and Ce (k) of CeO_2 /eGr.

The crystallite structure and composition of CeO_2 , eGr and CeO_2 /eGr composite (1:1 wt.) were evaluated by Raman spectra, XRD and XPS. In Raman spectra of Figure 2a, it shows a characteristic peak located at 461 cm^{-1} for the CeO_2 sample, which stems from the symmetrical stretching of Ce-O vibrational and originates from the F2g vibrational mode of the CeO_2 phase [33]. For eGr, the peaks at 1356 , 1580 and 2710 cm^{-1} were assigned to D, G and 2G bands of graphene, respectively [34]. The D band at $\sim 1356\text{ cm}^{-1}$ is derived from the defects and structural disorder in the sp^2 -carbon nanomaterials. The G band at 1580 cm^{-1} is related to the in-plane vibrations of the 2D hexagonal graphene lattice. The CeO_2 /eGr composite sample possesses both Raman characteristics of CeO_2 and eGr. XRD was used to analyze the structure of the prepared materials. In Figure 2b, the strong and sharp diffraction peaks indicate all the samples are in good crystallinity. For eGr, two diffraction peaks at 26.4° and 54.5° are observed, which are related to (002) and (004) planes of graphene, this is in accordance with the SEAD result (Figure 1e). For CeO_2 , the diffraction peaks located at 28.5° , 33.1° , 47.5° , 56.3° , 59.1° , 69.4° , 76.7° , 79.1° and 88.4° correspond to

(111), (200), (220), (311), (222), (400), (331), (420) and (422) planes (JCPDS 81-0792). The CeO₂/eGr composite also contains all the characteristic peaks of CeO₂ and eGr. Based on the CeO₂/eGr composite containing all the features of CeO₂ and eGr, the chemical composition of the CeO₂/eGr composite was further characterized by XPS. The XPS survey spectrum (Figure 2c) reveals the existence of Ce, O, and C elements in the CeO₂/eGr composite. The Ce3d electron core line was analyzed and is depicted in Figure 2d; it can be deconvoluted into eight peaks and labeled as v₀, v₁, v₂, v₃ (3d_{3/2} region), and u₀, u₁, u₂, u₃ (3d_{5/2} region). Peaks v₀, v₂, v₃ and u₀, u₂, u₃ are characteristics of Ce(IV) 3D final states, while, v₁ and u₁ are Ce(III) 3D final states [35]. Therefore, the as-prepared CeO₂ contains part of Ce(III), and the percentage of Ce(III) was calculated by Equation (1), which is based on the fitted areas of the corresponding peaks of Ce(III) and Ce(IV) [36].

$$\left(\text{Ce}^{3+}\right)_{\text{surf}} = \frac{\text{Ce(III)}}{\text{Ce(III)} + \text{Ce(IV)}} \quad (1)$$

The calculated percentage of Ce(III) is ~20%, which is similar to the previously reported CeO₂ nanomaterials [36]. The presence of Ce(III) indicates the formation of oxygen vacancies, which can provide catalytically active sites for the sensor. The O1s spectrum can be separated into three peaks as illustrated in Figure 2e, the peak located at ~529.9 eV corresponds to the crystal lattice oxygen in CeO₂. The peak located at 532.2 eV and 533.4 eV could be, respectively, related to the oxygen vacancies and the adsorbed oxygen on the composite [37,38]. The C1s spectrum can be separated into three peaks (Figure 2f). The peak placed at 284.6 eV corresponds to the sp² carbon atoms or can be attributed to C=C [39]. The other small peaks at 286.1 and 287.9 eV correspond to C–O and C=O on the surface of the composite, respectively.

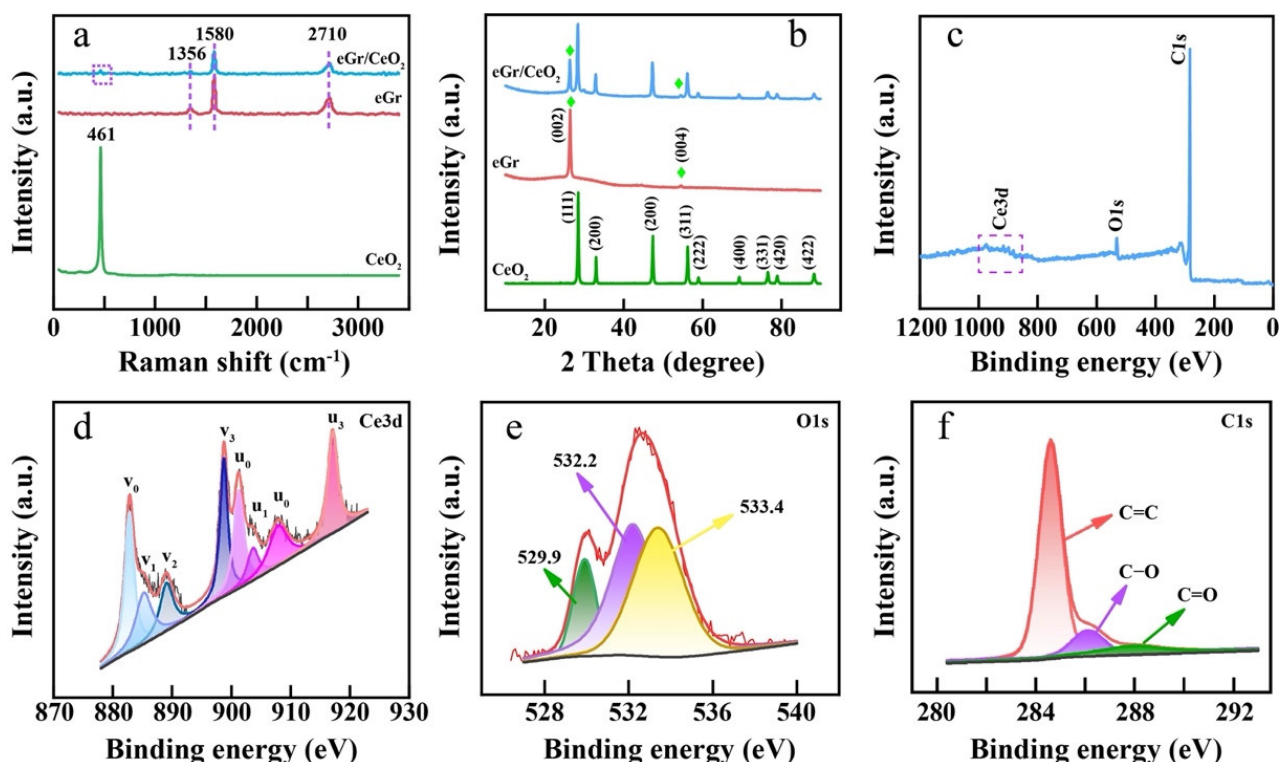


Figure 2. (a) Raman spectra, (b) XRD patterns of eGr, CeO₂, and CeO₂/eGr, (c) XPS survey spectrum, (d) Ce3d, (e) O1s and (f) C1s spectra of CeO₂/eGr composite, respectively.

3.2. The Electrochemical Characteristic of the Prepared Electrode

The prepared eGr, CeO₂, and CeO₂/eGr composites (1:1 wt.) were, respectively, cast on a glassy carbon electrode (eGr/GCE, CeO₂/GCE and CeO₂/eGr/GCE), and their elec-

trochemical performances were firstly estimated by Cyclic voltammetry (CV) at 50 mV s^{-1} in the solution of $5 \text{ mM } [\text{Fe}(\text{CN})_6]^{3-/4-}$ and 0.1 M KCl . The bare GCE electrode was conducted as the control sample. From Figure 3a, all electrodes show different levels of electrochemical activity, after evaluating the redox peak current densities and CV curve area, the electrochemically active follows the order of $\text{CeO}_2/\text{eGr}/\text{GCE} > \text{eGr}/\text{GCE} > \text{CeO}_2/\text{GCE} > \text{GCE}$. This suggests that the $\text{CeO}_2/\text{eGr}/\text{GCE}$ has the largest specific surface area, and the best electrochemically active and kinetic, which could arise from the synergistic effects of excellent catalytic active sites of CeO_2 and good electron transference of eGr. In addition, the standard heterogeneous rate constant (k^0) for bare GCE, $\text{CeO}_2/\text{eGr}/\text{GCE}$, eGr/GCE , CeO_2/GCE were calculated by Nicholson's equation [40] and the values are, respectively, $0.0041 \text{ cm}\cdot\text{s}^{-1}$, $0.0077 \text{ cm}\cdot\text{s}^{-1}$, $0.0045 \text{ cm}\cdot\text{s}^{-1}$, $0.0049 \text{ cm}\cdot\text{s}^{-1}$. The $\text{CeO}_2/\text{eGr}/\text{GCE}$ has the highest value of $0.0077 \text{ cm}\cdot\text{s}^{-1}$ that verifies CeO_2/eGr composite provides the best conditions for electron transfer.

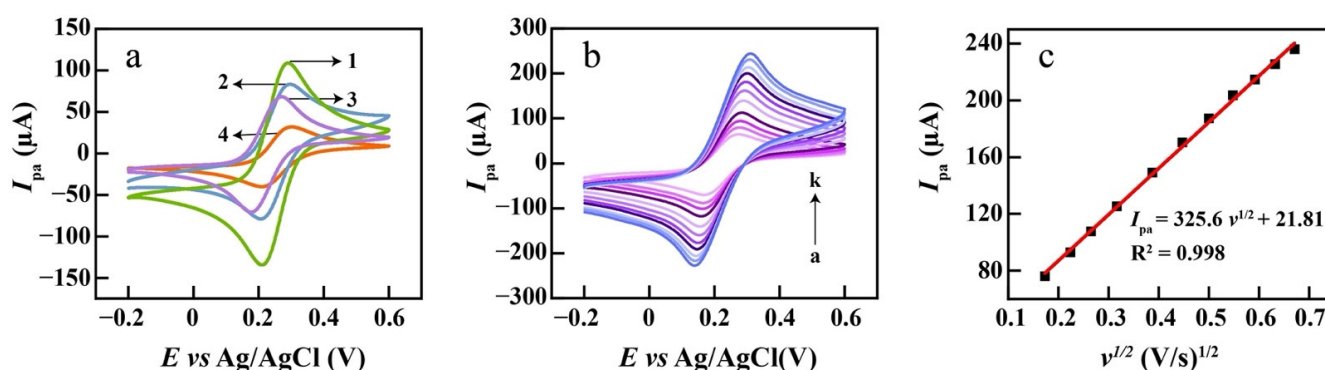


Figure 3. (a) CVs of $\text{CeO}_2/\text{eGr}/\text{GCE}$ in the presence of $5 \text{ mM } [\text{Fe}(\text{CN})_6]^{3-/4-}$ solution in aqueous 0.1 M KCl . $\text{CeO}_2/\text{eGr}/\text{GCE}$ (1), eGr/GCE (2), CeO_2/GCE (3), bare GCE (4); (b) CVs of $\text{CeO}_2/\text{eGr}/\text{GCE}$ in the presence of $5 \text{ mM } [\text{Fe}(\text{CN})_6]^{3-/4-}$ solution in aqueous 0.1 M KCl at various scan rate (from a to k): $0.03, 0.05, 0.07, 0.1, 0.15, 0.2, 0.25, 0.3, 0.35, 0.4, 0.45 \text{ V s}^{-1}$. (c) The plot of peak currents vs. $v^{1/2}$.

The electroactive surface area is a critical factor for the electrochemical sensor, which was estimated in $[\text{Fe}(\text{CN})_6]^{3-/4-}$ solution with scan rates ranging from 0.03 to 0.45 V s^{-1} via the Randles-Sevcik equation (Equation (2)) [41].

$$I_{pa} = (2.69 \times 10^5) n^{3/2} A D^{1/2} C v^{1/2} \quad (2)$$

where n refers to electron transfer number, A is the active surface area, C is the concentration of $[\text{Fe}(\text{CN})_6]^{3-/4-}$, v is the scan rate and D is the diffusion coefficient. Here, $n = 1$, $D = 6.6 \times 10^{-6} \text{ cm}^2 \text{ s}^{-1}$ [34] for $5 \text{ mM K}_3[\text{Fe}(\text{CN})_6]$ solution containing 0.1 M KCl . For $\text{CeO}_2/\text{eGr}/\text{GCE}$ (Figure 3b), the active surface area of $\text{CeO}_2/\text{eGr}/\text{GCE}$ was calculated to be 0.097 cm^2 (Figure 3c), which is higher than that of the electroactive surface areas of GCE (0.04 cm^2), eGr/GCE (0.08 cm^2), and CeO_2/GCE (0.045 cm^2), which is displayed in the Supporting Information, Figure S1. This result agrees well with the electrochemical activity order of the prepared sensors. The roughness factor (f_r) of the electrochemical sensors was calculated to evaluate the actual active surface area by comparing the oxidation peak current (I_{pa}) of the prepared sensor to bare GCE for $[\text{Fe}(\text{CN})_6]^{3-/4-}$ reaction [42]. Peaks ratio is equal to areas ratio according to the proposed Equation (3) [42].

$$f_r = \frac{I_{p2}}{I_{p1}} = \frac{A_2}{A_1} \quad (3)$$

The f_r determined by electrochemical methods depends not only on the size of the electrode (the actual surface), but also on the number of redox centers that can be reached on the surface. Therefore, the f_r was calculated to be 2.425 , 2 , and 1.625 for $\text{CeO}_2/\text{eGr}/\text{GCE}$, eGr/GCE , and CeO_2/GCE , respectively.

3.3. The Electrochemical Performance of the Prepared Electrode for 4-BPA Detection

The GCE, eGr/GCE, CeO₂/GCE and CeO₂/eGr/GCE (1:1 wt.) for 4-BPA detection were characterized by CV in the electrolyte with and without 50 μmol L⁻¹ 4-BPA in 0.1 mol L⁻¹ phosphate buffer (pH = 3). As displayed in Figure 4a, when the presence of 50 μmol L⁻¹ 4-BPA, all electrodes present one oxidation peak, which indicates the 4-BPA is electrochemically detectable and the reaction of 4-BPA is irreversible. The CeO₂/eGr/GCE (1:1 wt.) shows the highest oxidation peak current (*I*_{pa}) and the lowest onset potential; this verified that the CeO₂/eGr composite has the best sensitivity for electrochemical detection of 4-BPA, which should be attributed to the synergetic effect of the catalytic properties of CeO₂ and the fast electron transference of eGr. The ratios between CeO₂ and eGr have further been measured and shown in Figure 4b. With the CeO₂:eGr ratio increasing from 0:4 to 1:1, the oxidation peak current of 4-BPA increases and reaches the maximum at the ratio of 1:1, then the peak current drops with the further increase in the CeO₂ content. The reason could be that CeO₂ is a semiconductor, and it provides electrocatalytic activity sites. When the CeO₂ content is too low, it will not create enough activity sites. While the content is higher than 1:1, the conductivity and electron transference of the electrode will decrease. Therefore, the optimum ratio was 1:1 for 4-BPA detection and selected in the following study.

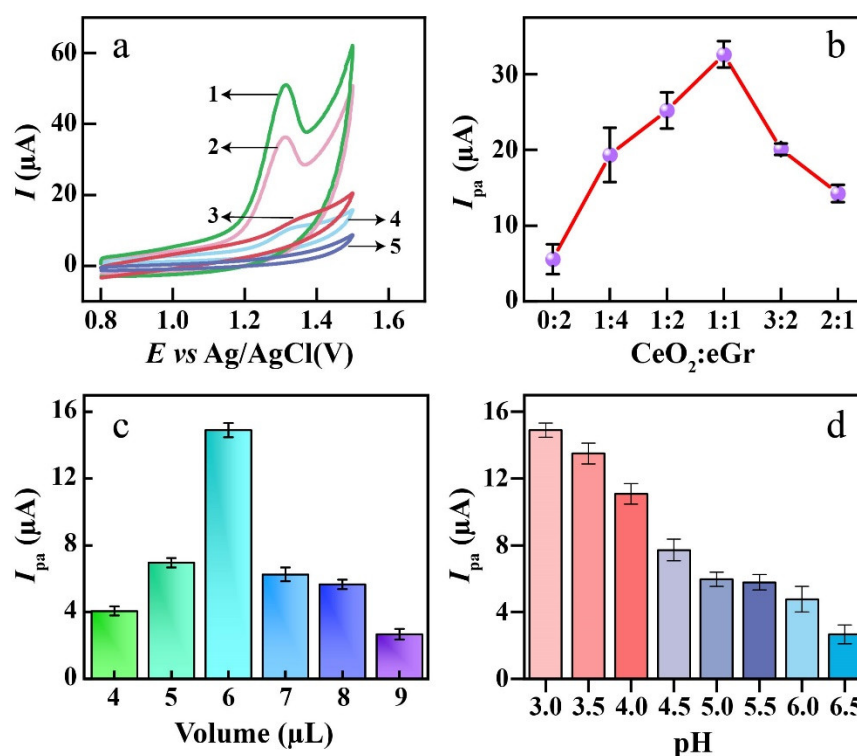


Figure 4. (a) CVs of CeO₂/eGr/GCE (1), eGr/GCE (2), bare GCE (3) and CeO₂/GCE (4) in 0.1 M PBS solution containing 50 μmol L⁻¹ 4-BPA at the scan rate of 100 mV s⁻¹, CeO₂/eGr/GCE (5) in PBS solution without 4-BPA; (b) Influence of the ratio between CeO₂ and eGr on the response of 4-BPA based on LSVs. (c) the response of 10 μmol L⁻¹ 4-BPA to different volumes of composite nanomaterial in PBS solution (pH = 3). (d) Influence of pH on the peak current of 4-BPA in 0.1 M PBS solution.

The different loading amounts of CeO₂/eGr composite on GCE were measured with 10 μmol L⁻¹ 4-BPA (Supporting information, Figure S2). It was found that the oxidation peak current of 4-BPA increases with the loading volume, increasing to 6 μL, while the response decreased when the loading amount further increased (Figure 4c). This could be due to the lack of cover on the electrode surface when the loading composites were below

6 μL , while too much loading amount would have hindered the activity sites that cause the decrease in the response peak current [43].

The PBS, Britton–Robison (B-R), and acetic acid-sodium acetate buffer solutions were evaluated as supporting electrolytes for 4-BPA detection (Supporting information, Figure S3). Among these supporting electrolytes, the PBS buffer solution shows more sensitivity for 4-BPA detection. Therefore, PBS was selected as a supporting electrolyte. Moreover, pH is another key impact factor for electrochemical analysis. The pH values ranging from 3 to 6.5 were evaluated in 0.1 M PBS buffer solution (Supporting information, Figure S4). It can be seen that the optimum response pH for 4-BPA was 3, and the response gradually decreased as the pH increased (Figure 4d). This phenomenon could be due to the conductivity loss and the presence of carboxyl groups with the increase in pH [44].

The oxidation process of 4-BPA on $\text{CeO}_2/\text{eGr}/\text{GCE}$ was further studied by linear sweep voltammogram (LSV); different scan rates (50 mV s^{-1} to 450 mV s^{-1}) were conducted and $20 \mu\text{mol L}^{-1}$ 4-BPA was used. As exhibited in Figure 5a, the I_{pa} increased when the scan rates increased. Moreover, the oxidation peaks positively shifted. More importantly, the oxidation peak current increased linearly with the square root of scan rates (Figure 5b), the linear regression is $I_{\text{pa}} = 3.936v^{1/2} - 9.318$, $R^2 = 0.999$ and the linear relationship for $\ln(I)$ versus $\ln(v)$ was established and the slope was found to be 0.82 (Supporting information, Figure S5), which indicates that the electrochemical oxidation of 4-BPA on $\text{CeO}_2/\text{eGr}/\text{GCE}$ was controlled by a mixed process [45]. The relationship between E_{pa} and $\ln v$ is presented by Laviron's theory [46]:

$$E_{\text{pa}} = E^0 + \left(\frac{RT}{\alpha nF} \right) \ln \left(\frac{RTk^0}{\alpha nF} \right) + \left(\frac{RT}{\alpha nF} \right) \ln v \quad (4)$$

where α is the charge transfer coefficient, E^0 is the apparent potential, n is the number of the electron, v is the scan rate, the values of R , T and F are $8.314 \text{ J K}^{-1} \text{ mol}^{-1}$, 298 K and 96485 C mol^{-1} , respectively. Therefore, the number of electrons can be calculated via the linear equations of $E_{\text{pa}} - \ln v$ (Supporting information, Figure S6). Generally, for an irreversible electrode process, the value of α is assumed to be 0.5. Hence, the value of n is calculated to be 2. Therefore, the electrocatalytic oxidation mechanism of 4-BPA is proposed in Figure 5c, where 4-BPA will firstly be degraded to 4-bromophenol. Then, the 4-bromophenol will be electrochemically oxidized to enzoquinone [47]. The whole process has two electrons involved, which is in accordance with the calculated results from Laviron's theory.

DPV shows the sensitive response to low concentrations as compared to LSV. Therefore, DPV was used to detect 4-BPA in PBS solution with different concentrations. As illustrated in Figure 5d, the peak current increases linearly with the concentrations of 4-BPA varying from 0.3 to $150 \mu\text{M}$. However, there are two linear relationships obtained. From Figure 5e, in the range of 0.3 to $20 \mu\text{M}$, the linear regression equation is $I_{\text{pa}} = 0.75c + 0.08$, ($R^2 = 0.991$), and from 20 to $150 \mu\text{M}$, the linear relationship is $I_{\text{pa}} = 0.199c + 11.24$, ($R^2 = 0.993$). Moreover, the lowest detection limit (LOD) was calculated to be $0.06 \mu\text{mol L}^{-1}$ according to the following equation of 3 s/m , where m is the slope of the regression equation and s is the standard deviation of the response.

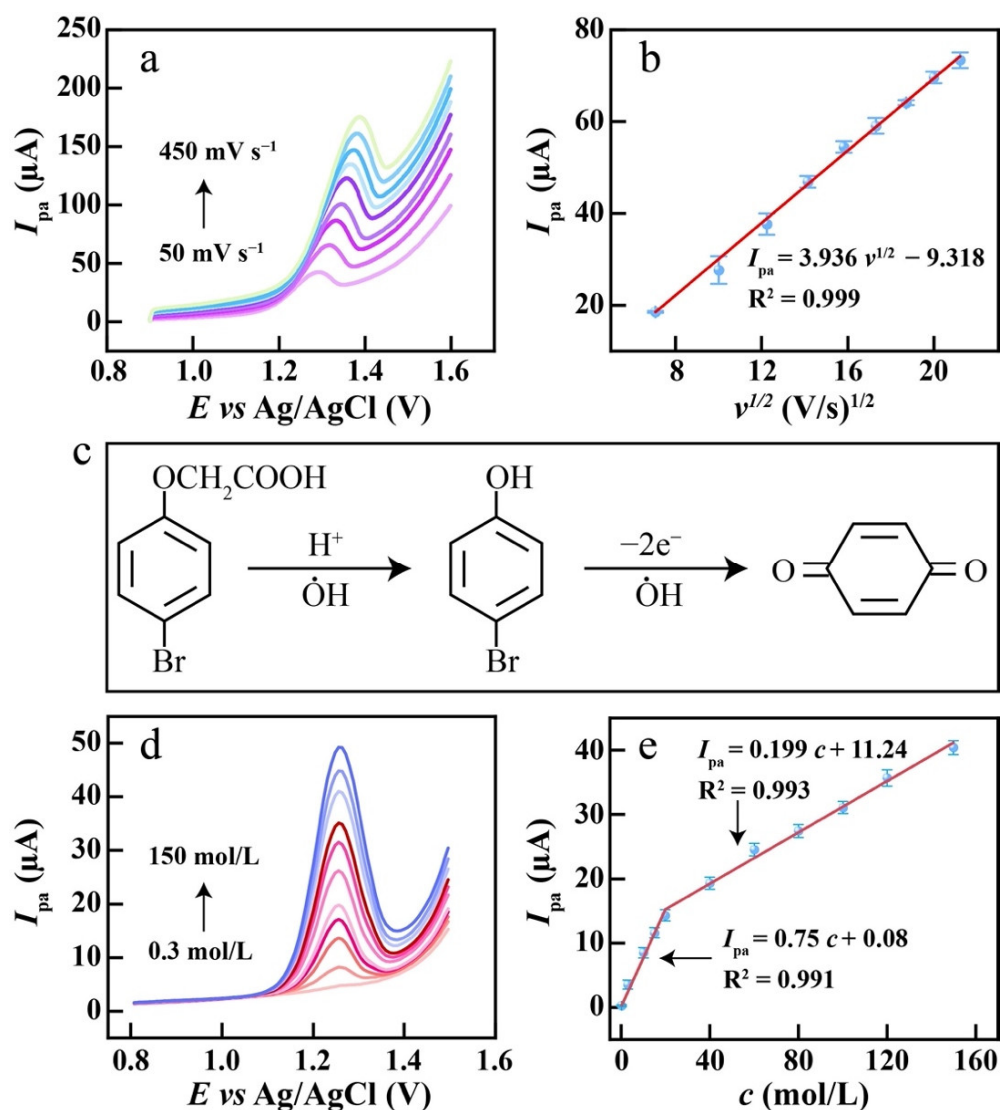


Figure 5. (a) LSVs of CeO₂/eGr/GCE in 0.1 M PBS solution containing 20 μmol L⁻¹ 4-BPA at 50, 100, 150, 200, 250, 300, 350, 400, 450 mV s⁻¹, (b) the plot of I_{pa} vs. $v^{1/2}$, (c) the proposed electrochemical reaction process of 4-BPA, (d) DPVs of CeO₂/eGr/GCE in 0.1 M PBS solution containing 0.3, 3, 10, 15, 20, 40, 60, 80, 100, 120, 150 μmol L⁻¹ 4-BPA, (e) the plot of the oxidation peak current vs. the concentration of 4-BPA.

3.4. The Repeatability and the Anti-Interference Ability of the CeO₂/eGr/GCE

The repeatability of the CeO₂/eGr/GCE was carried out with 10 μmol L⁻¹ 4-BPA by means of LSV (Supporting information, Figure S7). After 10 continuous measurements (Figure 6a), the relative standard deviation (RSD) of the oxidation peak currents was found to be 2.35% for 4-BPA. After storing the electrode at 4 °C for 15 days, the electroactive oxidation currents of 4-BPA reduced 3.21% compared to the original value. These results indicate that the proposed sensor has good stability and repeatability.

To estimate the anti-interference ability of the CeO₂/eGr/GCE, some regular interfering species were tested. From Figure 6b, no considerable interferences were observed in the presence of fifty-fold excess K⁺, Na⁺, Mg²⁺, glucose, sucrose, and ten-fold rutin, quercetin, fenitrothion, imidacloprid, clothianidin, IAA and SA (peak current change < 6%).

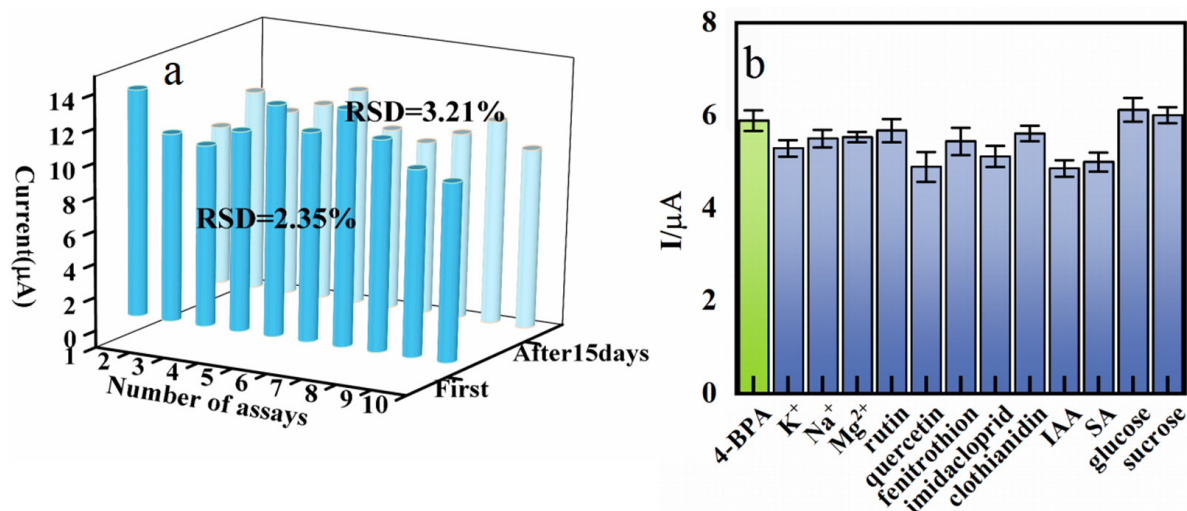


Figure 6. (a) The repeatability of current response for the $\text{CeO}_2/\text{eGr}/\text{GCE}$ in 0.1 M PBS (pH = 3) with 10 successive assays at first day and after 15 days. (b) The influence of other compounds on the detection of 4-BPA on $\text{CeO}_2/\text{eGr}/\text{GCE}$.

3.5. The Practical Application of the $\text{CeO}_2/\text{eGr}/\text{GCE}$

To evaluate the practicability of $\text{CeO}_2/\text{eGr}/\text{GCE}$, the sensor was used to detect 4-BPA in real apple samples; the analytical results are listed in Table 1. No response of 4-BPA was found in the apple sample, and the recoveries were evaluated by the standard addition method. The recoveries are in the range of 90–108%. This proposed CeO_2/eGr sensor shows great potential for the detection of plant growth regulators in the agricultural industry.

Table 1. Results of the recovery analysis of 4-BPA in apple sample ($n = 3$).

Sample	Added Value (μM)	Determined Value (μM)	Recovery (%)
1	0	Not detected (a, b)	-
2	0.5	0.45 ± 0.01	90%
3	1	1.08 ± 0.04	108%
4	3	2.78 ± 0.03	93%
5	5	4.86 ± 0.04	97%

a The 4-BPA level determined by the proposed $\text{CeO}_2/\text{eGr}/\text{GCE}$. b The 4-BPA level determined by the HPLC system.

4. Conclusions

In this work, we used an eco-friendly method of electrochemical exfoliation to prepare eGr and the hydrothermal method to prepare CeO_2 . Then, we constructed a selective, sensitive electrochemical method based on a eGr/CeO_2 composite and modified GCE to electrochemically detect 4-BPA. The prepared CeO_2/eGr sensor exhibited excellent electrocatalytic activity due to the synergistic effect of the excellent catalytic active sites of CeO_2 and good electron transference of the eGr. The developed CeO_2/eGr sensor has an active surface area of 0.097 cm^2 and a roughness factor of 2.425. The optimized ratio of $\text{CeO}_2:\text{eGr}$ is 1:1 for 4-BPA determination. The CeO_2/eGr sensor exhibited good linearity in a wide range from 0.3 to $150 \mu\text{mol/L}$ and the lowest detection limit of $0.06 \mu\text{mol/L}$ for 4-BPA detection. Electrochemical oxidation of 4-BPA followed a mix-controlled process, which involves $2e$ in the transference processes. In addition, there were no significant interfering substances among K^+ , Na^+ , Mg^{2+} , rutin, quercetin, fenitrothion, imidacloprid, clothianidin, IAA, SA, glucose, and sucrose. The proposed electrochemical sensor showed excellent repeatability with the RSD of 2.35% for 10 measurements. In addition, the recoveries of the proposed CeO_2/eGr sensor were evaluated by the standard addition method, and are in the range of 90–108%. The low cost and easily-made sensor has great potential for detecting other plant growth regulators.

Supplementary Materials: The following supporting information can be downloaded at: <https://www.mdpi.com/article/10.3390/bios12090760/s1>, Figure S1: the plot of peak currents vs. $v^{1/2}$ for (a) CeO₂/GCE, (b) GCE, (c) eGr/GCE in the presence of 5 mM [Fe(CN)₆]^{3−/4−} solution in aqueous of 0.1 M KCl. Figure S2: LSVs response of 10 μM 4-BAP to different volumes of composite in PBS solution (pH = 3). Figure S3: LSVs for 4-BPA detection in different buffer solution. Figure S4: Influence of pH on 4-BPA detection in 0.1 M PBS solution. Figure S5: the plots of $\ln I$ vs. $\ln v$ for 20 μM 4-BPA at 0.05, 0.1, 0.15, 0.2, 0.25, 0.3, 0.35, 0.4, 0.45 V s^{−1}. Figure S6: the plots of E_{pa} vs. $\ln v$ for 20 μM 4-BPA at 0.05, 0.1, 0.15, 0.2, 0.25, 0.3, 0.35, 0.4, 0.45 V s^{−1}. Figure S7: (a) The LSVs of the CeO₂/eGr/GCE in 0.1 M PBS (pH = 3) at first day and after 15 days. (b) 10 continuous measurements of 4-BPA on CeO₂/eGr/GCE.

Author Contributions: Conceptualization, project administration, and funding acquisition, H.D., Y.Y. and Z.L.; methodology and data curation, Y.Z.; validation and formal analysis, X.W. and H.H.; investigation, J.A., H.Z. and X.Y.; writing—original draft preparation, H.D. and Y.Z.; writing—review and editing, Y.Y. and Z.L. All authors have read and agreed to the published version of the manuscript.

Funding: This research was funded by the National Natural Science Foundation of China (No. 51801039, 81860701, 82060714, 22104102), Guizhou Provincial Science and Technology Projects (NO. ZK [2021]242), The Innovation Team Project of Guizhou Higher Education ([2022]013), The open project of Laboratory of Xinjiang Native Medicinal and Edible Plant Resources Chemistry (NO. KSUZSYS202104). Sichuan Science and Technology Program (Grant No. 2021YJ0316).

Institutional Review Board Statement: Not applicable.

Informed Consent Statement: Not applicable.

Data Availability Statement: Not applicable.

Conflicts of Interest: The authors declare no conflict of interest.

References

1. Bons, H.K.; Kaur, M. Role of plant growth regulators in improving fruit set, quality and yield of fruit crops: A review. *J. Horticult. Sci. Biotechnol.* **2019**, *95*, 137–146. [[CrossRef](#)]
2. Kahlina, K.V.; Jurić, S.; Marijan, M.; Mutaliyeva, B.; Khalus, S.V.; Prosyaniuk, A.V.; Vinceković, M. Synthesis, Characterization, and Encapsulation of Novel Plant Growth Regulators (PGRs) in Biopolymer Matrices. *Int. J. Mol. Sci.* **2021**, *22*, 1847. [[CrossRef](#)] [[PubMed](#)]
3. Wei, Y.Z.; Zhang, H.N.; Li, W.C.; Xie, J.H.; Wang, Y.C.; Liu, L.Q.; Shi, S.Y. Phenological growth stages of lychee (*Litchi chinensis* Sonn.) using the extended BBCH-scale. *Sci. Horticult.* **2013**, *161*, 273–277. [[CrossRef](#)]
4. Fan, Y.X.; Yang, W.; Yan, Q.Q.; Chen, C.R.; Li, J.H. Genome-Wide Identification and Expression Analysis of the Protease Inhibitor Gene Families in Tomato. *Genes* **2020**, *11*, 1. [[CrossRef](#)] [[PubMed](#)]
5. Brondi, S.H.G.; Lanças, F.M. Development and validation of a multi-residue analytical methodology to determine the presence of selected pesticides in water through liquid chromatography. *J. Braz. Chem. Soc.* **2005**, *16*, 650–654. [[CrossRef](#)]
6. Rostami, S.; Azhdarpoor, A. The application of plant growth regulators to improve phytoremediation of contaminated soils: A review. *Chemosphere* **2019**, *220*, 818–827. [[CrossRef](#)]
7. Sutcharitchan, C.; Miao, S.; Li, W.T.; Liu, J.M.; Zhou, H.; Ma, Y.X.; Ji, S.; Cui, Y.J. High performance liquid chromatography-tandem mass spectrometry method for residue determination of 39 plant growth regulators in root and rhizome Chinese herbs. *Food Chem.* **2020**, *322*, 126766. [[CrossRef](#)]
8. Chen, H.; Feng, X.; Guo, H.S.; Zhang, H.W. Simultaneous determination of phytohormones containing carboxyl in crude extracts of fruit samples based on chemical derivatization by capillary electrophoresis with laser-induced fluorescence detection. *J. Chromatogr. B* **2011**, *879*, 1802–1808. [[CrossRef](#)]
9. Jiang, C.L.; Dai, J.X.; Han, H.L.; Wang, C.; Li, Z.; Lu, C.Y.; Chen, H.P. Determination of thirteen acidic phytohormones and their analogues in tea (*Camellia sinensis*) leaves using ultra high performance liquid chromatography tandem mass spectrometry. *J. Chromatogr. B* **2020**, *1149*, 122144. [[CrossRef](#)]
10. Qin, G.F.; Zou, K.T.; Tian, L.; Li, Y.B. Determination of Five Plant Growth Regulator Containing Carboxyl in Bean Sprouts Based on Chemical Derivatization by GC-MS. *Food Anal. Methods* **2018**, *11*, 2628–2635. [[CrossRef](#)]
11. Arduini, F.; Cinti, S.; Caratelli, V.; Amendola, L.; Palleschi, G.; Moscone, D. Origami multiple paper-based electrochemical biosensors for pesticide detection. *Biosens. Bioelectron.* **2019**, *126*, 346–354. [[CrossRef](#)]
12. Fusco, G.; Gallo, F.; Tortolini, C.; Bollella, P.; Ietto, F.; Mico, A.D.; D'Annibale, A.; Antiochia, R.; Favero, G.; Mazzei, F. AuNPs-functionalized PANABA-MWCNTs nanocomposite-based impedimetric immunosensor for 2,4-dichlorophenoxy acetic acid detection. *Biosens. Bioelectron.* **2017**, *93*, 52–56. [[CrossRef](#)]

13. Liu, F.P.; Qin, X.W.; Huang, Z.F.; Zhang, G.; Xiang, C.Z.; Zhang, C.Y.; Liang, H.L.; Peng, J.Y. Green synthesis of porous graphene and its application for sensitive detection of hydrogen peroxide and 2,4-dichlorophenoxyacetic acid. *Electrochim. Acta.* **2019**, *295*, 615–623. [[CrossRef](#)]
14. Skrzypczyńska, K.; Kuśmierk, K.; Świątkowski, A. Carbon paste electrodes modified with various carbonaceous materials for the determination of 2,4-dichlorophenoxyacetic acid by differential pulse voltammetry. *J. Electroanal. Chem.* **2016**, *766*, 8–15. [[CrossRef](#)]
15. Wang, H.M.; Xu, Q.; Wang, J.; Du, W.; Liu, F.P.; Hu, X.Y. Dendrimer-like amino-functionalized hierarchical porous silica nanoparticle: A host material for 2,4-dichlorophenoxyacetic acid imprinting and sensing. *Biosens. Bioelectron.* **2018**, *100*, 105–114. [[CrossRef](#)]
16. Arvand, M.; Gaskarmahalleh, A.A.; Hemmati, S. Enhanced-Oxidation and Highly Sensitive Detection of Tartrazine in Foodstuffs via New Platform Based on Poly(5-Sulfosalicylic Acid)/Cu(OH)₂ Nanoparticles. *Food Anal. Methods* **2017**, *10*, 2241–2251. [[CrossRef](#)]
17. Su, D.D.; Zhang, Y.Y.; Wang, Z.J.; Wan, Q.J.; Yang, N.J. Decoration of graphene nano platelets with gold nanoparticles for voltammetry of 4-nonylphenol. *Carbon* **2017**, *117*, 313–321. [[CrossRef](#)]
18. Arumugasamy, S.K.; Govindaraju, S.; Yun, K. Electrochemical sensor for detecting dopamine using graphene quantum dots incorporated with multiwall carbon nanotubes. *Appl. Surf. Sci.* **2020**, *508*, 145294. [[CrossRef](#)]
19. Kim, C.K.; Kim, T.; Choi, I.Y.; Soh, M.; Kim, D.H.; Kim, Y.J.; Jang, H.D.; Yang, H.S.; Kim, J.Y.; Park, H.K.; et al. Rücktitelbild: Ceria Nanoparticles that can Protect against Ischemic Stroke. *Chem. Int. Ed. Eng.* **2012**, *51*, 11039–11043. [[CrossRef](#)]
20. Wang, Z.L.; Li, G.R.; Ou, Y.N.; Feng, Z.P.; Qu, D.L.; Tong, Y.X. Electrochemical deposition of Eu³⁺-doped CeO₂ nanobelts with enhanced optical properties. *J. Phys. Chem. C* **2011**, *115*, 351–356. [[CrossRef](#)]
21. Ansari, A.A.; Alam, M. Nickle-ion-substituted ceria nanoparticles-based electrochemical sensor for sensitive detection of thiourea. *J. Mater. Sci.* **2021**, *32*, 23266–23274. [[CrossRef](#)]
22. Chen, C.H.; Yang, S.W.; Chuang, M.C.; Woon, W.Y.; Su, C.Y. Towards the continuous production of high crystallinity graphene via electrochemical exfoliation with molecular in situ encapsulation. *Nanoscale* **2015**, *7*, 15362–15373. [[CrossRef](#)]
23. Ambrosi, A.; Chua, C.K.; Latiff, N.M.; Loo, A.H.; Wong, C.H.A.; Eng, A.Y.S.; Bonanni, A.; Pumera, M. Graphene and its electrochemistry—an update. *Chem. Soc. Rev.* **2010**, *39*, 4146–4157. [[CrossRef](#)]
24. Pumera, M. Electrochemistry of graphene, graphene oxide and other graphenoids: Review. *Electrochem. Commun.* **2013**, *36*, 14–18. [[CrossRef](#)]
25. Ambrosi, A.; Chua, C.K.; Bonanni, A.; Pumera, M. Electrochemistry of Graphene and Related Materials. *Chem. Rev.* **2014**, *114*, 7150–7188. [[CrossRef](#)]
26. Brownson, D.A.C.; Banks, C.E. *The Handbook of Graphene Electrochemistry*, 1st ed; Springer: London, UK, 2014; pp. 6–20. [[CrossRef](#)]
27. Jayaprakash, G.K. Pre-post redox electron transfer regioselectivity at the alanine modified nano graphene electrode interface. *Chem. Phys. Lett.* **2022**, *789*, 139295. [[CrossRef](#)]
28. Sun, J.J.; Xie, X.H.; Xie, K.; Xu, S.C.; Jiang, S.Z.; Ren, J.F.; Zhao, Y.F.; Xu, H.Q.; Wang, J.J.; Yue, W.W. Magnetic Graphene Field-Effect Transistor Biosensor for Single-Strand DNA Detection. *Nanoscale Res. Lett.* **2019**, *14*, 248. [[CrossRef](#)]
29. Liu, Y.; Qiu, Z.P.; Wan, Q.J.; Wang, Z.H.; Wu, K.B.; Yang, N.J. High-Performance Hydrazine Sensor Based on Graphene Nano Platelets Supported Metal Nanoparticles. *Electroanalysis* **2016**, *28*, 126–132. [[CrossRef](#)]
30. Li, C.; Zhang, Y.Y.; Zeng, T.; Chen, X.Y.; Wang, W.Q.; Wan, Q.J.; Yang, N.J. Graphene nanoplatelet supported CeO₂ nanocomposites towards electrocatalytic oxidation of multiple phenolic pollutant. *Anal. Chim. Acta* **2019**, *1088*, 45–53. [[CrossRef](#)]
31. Zhang, Y.; Ai, J.X.; Hu, H.L.; Wang, X.; Zhou, H.X.; Du, K.Z.; Du, H.J.; Yang, Y. Highly Sensitive Detection of Kinetin with Electrochemical Exfoliation of Graphene Nanosheets. *Appl. Phys. A* **2022**, *128*, 350. [[CrossRef](#)]
32. Kumar, A.A.; Swamy, B.E.K.; Rani, T.S.; Ganesh, P.S.; Raj, Y.P. Voltammetric determination of catechol and hydroquinone at poly(murexide) modified glassy carbon electrode. *Mater. Sci. Eng. C* **2019**, *98*, 746–752. [[CrossRef](#)] [[PubMed](#)]
33. Tan, H.Y.; Wang, J.; Yu, S.Z.; Zhou, K.B. Support Morphology-Dependent Catalytic Activity of Pd/CeO₂ for Formaldehyde Oxidation. *Sci. Technol.* **2015**, *49*, 8675–8682. [[CrossRef](#)] [[PubMed](#)]
34. Yu, J.; Zhang, Y.Y.; Li, H.; Wan, Q.J.; Li, Y.W.; Yang, N.J. Electrochemical properties and sensing applications of nanocarbons: A comparative study. *Carbon* **2018**, *129*, 301–309. [[CrossRef](#)]
35. Mullins, D.R.; Overbury, S.H.; Huntley, D.R. Electron spectroscopy of single crystal and polycrystalline cerium oxide surfaces. *Surf. Sci.* **1998**, *409*, 307–319. [[CrossRef](#)]
36. Lyu, L.; Xie, Q.; Yang, Y.Y.; Wang, R.R.; Cen, W.F.; Luo, S.Y.; Yang, W.S.; Gao, Y.; Xiao, Q.Q.; Zou, P.; et al. A Novel CeO₂ Hollow-Shell Sensor Constructed for High Sensitivity of Acetone Gas Detection. *Appl. Surf. Sci.* **2022**, *571*, 151337. [[CrossRef](#)]
37. Meng, F.M.; Wang, L.N.; Cui, J.B. Controllable synthesis and optical properties of nano-CeO₂ via a facile hydrothermal route. *J. Alloys Compd.* **2013**, *556*, 102–108. [[CrossRef](#)]
38. Yang, Y.; Yang, Y.M.; Fu, T.W.; Zhu, J.; Fan, J.P.; Zhang, Z.; Zhang, J.Q. Influence of ethanol content in the precursor solution on anodic electrodeposited CeO₂ thin films. *Thin Solid Film.* **2014**, *556*, 128–136. [[CrossRef](#)]
39. Parvez, K.; Wu, Z.S.; Li, R.; Liu, X.; Graf, R.; Feng, X.; Müllen, K. Exfoliation of Graphite into Graphene in Aqueous Solutions of Inorganic Salts. *J. Am. Chem. Soc.* **2014**, *136*, 6083–6091. [[CrossRef](#)]
40. Nicholson, R.S. Theory and Application of Cyclic Voltammetry for Measurement of Electrode Reaction Kinetics. *Anal. Chem.* **1965**, *37*, 1351–1355. [[CrossRef](#)]

41. Sha, T.; Liu, J.; Sun, M.; Li, L.; Bai, J.; Hu, Z.; Zhou, M. Green and low-cost synthesis of nitrogen-doped graphene-like mesoporous nanosheets from the biomass waste of okara for the amperometric detection of vitamin C in real samples. *Talanta* **2019**, *200*, 300–306. [[CrossRef](#)]
42. Krzyczmonik, P.; Socha, E.; Skrzypek, S.; Soliwoda, K.; Celichowski, G.; Grobelny, J. Honeycomb-structured porous poly(3,4-ethylenedioxythiophene) composite layers on a gold electrode. *Thin Solid Films* **2014**, *565*, 54–61. [[CrossRef](#)]
43. Zamiri, R.; Salehizadeh, S.A.; Ahangar, H.A.; Shabani, M.; Rebelo, A.; Ferreira, J.M.F. Dielectric and optical properties of Ni-and Fe-doped CeO₂ Nanoparticles. *Appl. Phys. A* **2019**, *125*, 1–7. [[CrossRef](#)]
44. Chen, Y.N.; Chen, Q.; Zhao, H.; Dang, J.Q.; Jin, R.; Zhao, W.; Li, Y.H. Wheat Straws and Corn Straws as Adsorbents for the Removal of Cr(VI) and Cr(III) from Aqueous Solution: Kinetics, Isotherm, and Mechanism. *ACS Omega* **2020**, *5*, 6003–6009. [[CrossRef](#)]
45. Huang, Q.; Lin, X.; Tong, L.; Tong, Q.X. Graphene Quantum Dots/Multiwalled Carbon Nanotubes Composite-Based Electrochemical Sensor for Detecting Dopamine Release from Living Cells. *ACS Sustain. Chem. Eng.* **2020**, *8*, 1644–1650. [[CrossRef](#)]
46. Laviron, E. General expression of the linear potential sweep voltammogram in the case of diffusionless electrochemical systems. *J. Electroanal. Chem.* **1979**, *101*, 19–28. [[CrossRef](#)]
47. Xu, D.D.; Song, X.Z.; Qi, W.Z.; Wang, H.; Bian, Z.Y. Degradation mechanism, kinetics, and toxicity investigation of 4-bromophenol by electrochemical reduction and oxidation with Pd-Fe/graphene catalytic cathodes. *Chem. Eng. J.* **2018**, *333*, 477–485. [[CrossRef](#)]